PHYSICAL REVIEW B **83**, 121312(R) (2011)

Photoexcitation of valley-orbit currents in (111)-oriented silicon metal-oxide-semiconductor field-effect transistors

J. Karch,[1] S. A. Tarasenko,[2] E. L. Ivchenko,[2] J. Kamann,[1] P. Olbrich,[1] M. Utz,[1] Z. D. Kvon,[3] and S. D. Ganichev[1]

[1]*Terahertz Center, University of Regensburg, D-93040 Regensburg, Germany*

[2]*Ioffe Physical-Technical Institute, Russian Academy of Sciences, 194021 St. Petersburg, Russia*

[3]*Institute of Semiconductor Physics, Russian Academy of Sciences, 630090 Novosibirsk, Russia*

(Received 7 March 2011; published 25 March 2011)

We demonstrate the injection of pure valley-orbit currents in multivalley semiconductors and present the phenomenological theory of this effect. We studied photoinduced transport in (111)-oriented silicon metal-oxide-semiconductor field effect transistors at room temperature. By shining circularly polarized light on exact oriented structures with six equivalent valleys, nonzero electron fluxes within each valley are generated, which compensate each other and do not yield a net electric current. By disturbing the balance between the valley fluxes, we demonstrate that the pure valley-orbit currents can be converted into a measurable electric current.

DOI: 10.1103/PhysRevB.83.121312 PACS number(s): 78.40.Fy, 72.40.+w, 73.40.Qv, 78.20.−e

Free carriers in solids can carry both positive and negative electric charge, which builds the basis for bipolar electronics. In addition, they possess degrees of freedom related to spin or valley degeneracy, the latter being relevant in multivalley semiconductors. The degeneracies enable one to engineer various distributions of carriers in the momentum, spin, and valley spaces. A controllable way of occupying a particular spin state or filling a particular valley is a key ingredient, respectively, for spintronics[1] or valleytronics[2,3] aimed at the development of novel solid-state devices. The candidates appropriate for the realization of valleytronic concepts include multivalley semiconductors such as silicon,[2,4] graphene,[3,5,6] and carbon nanotubes.[2] A remarkable selective population of the electron states is achieved by optical pumping with polarized light: circularly for spin polarization[7] and linearly polarized for "valley polarization."[8] Besides the selective valley population, the radiation can also cause a particle flux $\boldsymbol{i}_\nu$ within each valley, whose direction and magnitude depend on the valley number ν. In general, the total electric current $\boldsymbol{j} = e\sum_\nu \boldsymbol{i}_\nu$ is nonzero, measurable by conventional electric methods. However, for special geometries and light polarizations, the partial fluxes $\boldsymbol{i}_\nu$ do exist but the total electric current vanishes. This is the pure valley-orbit current proposed in Ref. 2 and implying the device's potential use of the valley index in analogy to the pure spin currents in spintronics and topological electronics.[9–14]

Here we report on the vivid evidence of the existence of pure valley-orbit currents and demonstrate that the individual control of electron fluxes in valleys can be achieved by the excitation of (111)-oriented Si-metal-oxide-semiconductor (Si-MOS) structures with polarized light. Such two-dimensional systems contain six equivalent electron valleys[4,15] (Fig. 1) and possess the overall point-group symmetry C_{3v}, that is, they are invariant with respect to the rotation by an angle of 120°. The irradiation of (111)-oriented Si-MOS structures leads to an emergence of the fluxes $\boldsymbol{i}_\nu$ in all six valleys [Fig. 1(a)]. The generation of the fluxes $\boldsymbol{i}_\nu$ is microscopically caused by the low symmetry of individual valleys [Fig. 1(b)] and stems from asymmetric electron photoexcitation. It is mostly of orbital origin while spin-related mechanisms are negligible due to the vanishingly small spin-orbit coupling in silicon. Owing to the mass anisotropy in valleys of bulk silicon and to the valley tilting with respect to the channel normal in (111) structures, the in-plane and out-of-plane motions of carriers are coupled. Therefore, the rates of optical transitions induced by radiation polarized in the channel plane depend on the electron wave vectors. Such an asymmetry of photoexcitation in the momentum space results in a polarization-dependent electron flux $\boldsymbol{i}_\nu$. This mechanism of current generation is similar to those considered in Refs. 16–19, but out of scope of this work and will be described elsewhere.

Instead, we focus on the distribution of the fluxes $\boldsymbol{i}_\nu$ over the valleys forming the pure valley-orbit currents or, under certain conditions, an electric current. A symmetry analysis shows that circularly polarized light normally incident upon the sample induces helicity-sensitive intravalley fluxes $\boldsymbol{i}_\nu^c$ in the directions perpendicular to the principal valley axes resulting in a zero net photocurrent [Fig. 1(c)]. On the other hand, the theory allows the generation of a total electric current by linearly polarized radiation [Fig. 1(d)]. Thus, first experimental evidence of valley-orbit currents in (111) Si-MOS structures is the lack of a net photocurrent for circularly and its observation for linearly polarized light. A further confirmation is the appearance of a photocurrent in samples with broken equivalence of valleys, for example, in miscut structures.

To verify the theoretical predictions we have experimentally studied photocurrents in MOS field-effect transistors (MOSFETs) fabricated on exact and miscut (111) silicon surfaces by means of standard MOS technology including preparation of SiO_2 with a thickness of 100 nm by high-temperature oxidation of silicon, preparation of heavily doped n^{++} contacts by ion implantation, and the fabrication of heavily doped polycrystalline semitransparent gates. The studied Si samples with the surface precisely oriented along the (111) plane contain two transistors [see inset of Fig. 2(a)] each prepared with a channel length of 1.5 mm, a width of 0.5 mm, and the channel directions parallel either to $x \parallel [\bar{1}10]$ or $y \parallel [\bar{1}\bar{1}2]$. A variation of the gate voltage V_g from 5 to 20 V changes the carrier density N_s from 1.0 to 4.1×10^{12} cm^{-2}. The sixfold degeneracy of our (111)-oriented Si has been previously approved in experiments on the phonon drag effect.[20] Note also that the energy of valley splitting, if any, in

 ©2011 American Physical Society

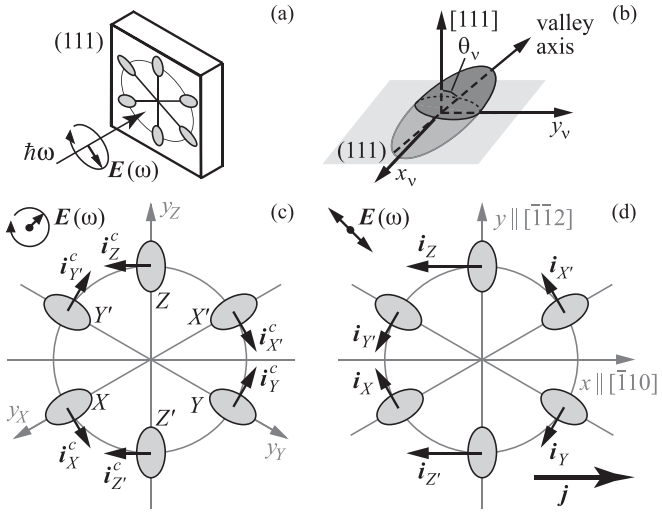

FIG. 1. (a) Excitation of (111)-oriented Si-MOS structures with, e.g., circularly polarized light. (b) Orientation of an individual valley. (c) Distribution of helicity-dependent fluxes over valleys induced in the exact (111) Si-MOSFET by normally incident light. The fluxes $\boldsymbol{i}_v^c$ are calculated after Eq. (4) based on symmetry arguments and determined by the coefficient A. They are directed perpendicularly to the valley principal axes and compensate each other to nullify the net electric current. The in-plane coordinates y_v attached to the valleys X, Y, and Z are shown. (d) Intravalley fluxes under excitation with linearly polarized light, the total current $\boldsymbol{j} = e\sum_v \boldsymbol{i}_v \neq 0$. The directions and magnitudes of fluxes in valleys are calculated after Eq. (4) for a particular case of $C = D = 0$. However, we emphasize that the choice of parameters does not affect the polarization dependence of the total current $\boldsymbol{j}$ [see Eq. (7)].

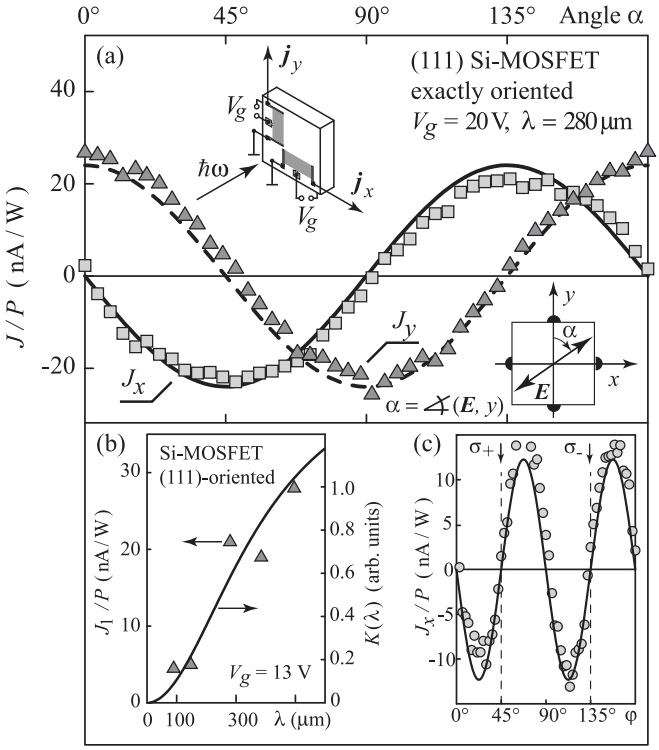

FIG. 2. (a) Photocurrent as function of the azimuth angle α measured in the precisely (111)-oriented MOSFET. Lines are fits to Eqs. (1) with one fitting parameter χ. The upper inset shows the experimental geometry and the lower the definition of the angle α with respect to the sample orientation. (b) Comparison of the wavelength dependencies of the linear photocurrent $J_1 = [J_y(\alpha = 0°) - J_y(\alpha = 90°)]/2 \propto \chi$ (triangles) and the calculated coefficient of free carrier absorption (solid curve). (c) Helicity dependence of the photocurrent, full line is a fit to Eq. (2).

nominally unstrained Si-MOSFETs is much smaller than the mean kinetic energy of carriers at room temperature and, thus, is negligible.[21] Another set of MOSFETs is fabricated on Si surfaces with the normal $\boldsymbol{n}$ rotated from the (111) orientation around the axis $x' = x \parallel [\bar{1}10]$ by an angle of $\delta\Theta = 4°$. Two transistors with the same size are prepared on the miscut substrate with the channels oriented either along x' or along the inclination axis $y' \perp \boldsymbol{n}, x'$ (see inset in Fig. 3). They have 70-nm thick SiO_2 layers and semitransparent polycrystalline Si gates. Variation in V_g from 5 to 20 V changes N_s from 1.4 to 5.7×10^{12} cm^{-2}. All used MOSFETs exhibit room-temperature electron mobilities μ in the channel between 400 and 800 cm^2/V s and typical energy separations of the first and second size quantized subbands ε_{21} from about 16 to 30 meV.[22] The orientation of the Si surfaces has been proved applying an x-ray diffractometer. The accuracy of the orientation is better than 0.5°.

For optical excitation we use an optically pumped terahertz molecular laser with NH_3, D_2O, and CH_3F as active gases.[23,24] Radiation with a pulse length of 100 ns and a peak power $P \sim 10$ kW is obtained at the wavelengths $\lambda = 90$, 148, 280, 385, and 496 μm corresponding to photon energies $\hbar\omega$ between 13.7 and 2.5 meV, being smaller than ε_{21}. The experimental geometries are illustrated in the insets of Figs. 2 and 3. All experiments are performed at room temperature applying normally incident radiation, which induces indirect Drude-like optical transitions in the Si-MOSFETs. Various polarization states of the radiation are achieved by transmitting the laser beam through $\lambda/2$ or $\lambda/4$ crystal quartz plates. By applying the $\lambda/2$ plates, we vary the azimuth angle α between the polarization plane of the radiation and the y (or y') axis [see the inset of Fig. 2(a)]. By applying $\lambda/4$ plates we produce elliptically polarized radiation, where the polarization state is determined by the angle φ between the y (or y') axis and the optical axis of the plate. The Stokes parameters $\mathcal{S} = e_x e_y^* + e_y e_x^*$, $\mathcal{C} = |e_x|^2 - |e_y|^2$ and the degree of circular polarization $P_{\rm circ}$ defined by $\mathrm{i}[\boldsymbol{e} \times \boldsymbol{e}^*] = (\boldsymbol{q}/q)P_{\rm circ}$ depend on the angles α and φ as follows: $\mathcal{S}(\alpha) = \sin 2\alpha$, $\mathcal{C}(\alpha) = -\cos 2\alpha$, $\mathcal{S}(\varphi) = (1/2)\sin 4\varphi$, $\mathcal{C}(\varphi) = -\cos^2 2\varphi$, and $P_{\rm circ} = \sin 2\varphi$. Here $\boldsymbol{e}$ is the polarization unit vector $\boldsymbol{E}/|\boldsymbol{E}|$ and $\boldsymbol{q}$ the photon wave vector directed along $-z$. The photocurrents are measured between source and drain contacts of the unbiased transistors via the voltage drop across a 50 Ω load resistor. Further details on the experimental technique can be found in Ref. 25.

Irradiating the exact (111) Si-MOSFETs with linearly polarized terahertz radiation at normal incidence generates photocurrent signals with a temporal shape reproducing the laser pulse. The signal rises monotonously with increasing gate voltage and, correspondingly, carrier density in the channel (not shown), as expected for Drude absorption.[17,19]

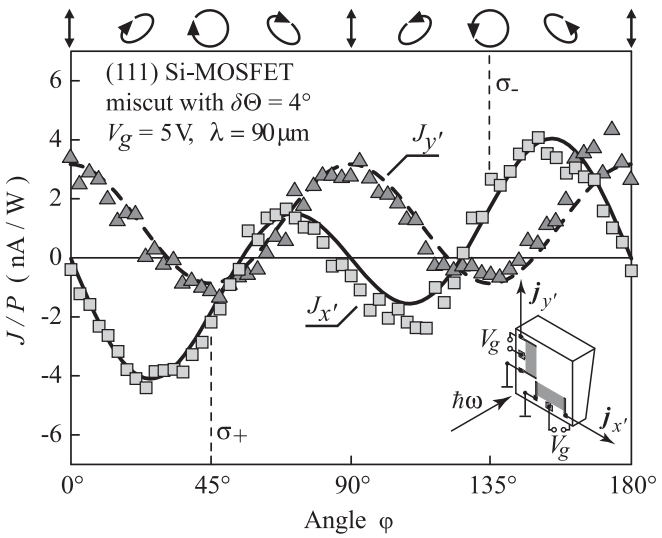

FIG. 3. Photocurrent as a function of the angle φ measured in the transistors prepared on the miscut surface. Lines are fits to Eqs. (3). The inset shows the experimental geometry. On top, the polarization ellipses corresponding to various angles φ are illustrated.

The dependencies on the azimuth angle α shown in Fig. 2(a) are well fitted by

$$J_x(\alpha) = \chi \sin 2\alpha, \quad J_y(\alpha) = -\chi \cos 2\alpha \tag{1}$$

with the same prefactor χ, in agreement with the theoretical expectation for the point group C_{3v} [see Eq. (7)]. In reference MOSFETs prepared on exact (001) Si surfaces, no signal has been detected for normal incidence.[17] Triangles in Fig. 2(b) show that, as expected for free-carrier absorption, the signal rises with increasing wavelength following the Drude formula of high-frequency conductivity.[18,25]

The variation of the photocurrent with the angle φ presented in Fig. 2(c) clearly demonstrates that the current vanishes for circularly polarized photoexcitation, σ_+ and σ_-, realized at $\varphi = 45^\circ$ and 135°. The best fit of the dependencies $J_x(\varphi)$ and $J_y(\varphi)$ (not shown) contains no contributions from $P_{\rm circ}$ and reduces to

$$J_x(\varphi) = \frac{\chi}{2} \sin 4\varphi, \quad J_y(\varphi) = -\chi \cos^2 2\varphi \tag{2}$$

with the same coefficient χ as in Eq. (1).

In the miscut samples, by contrast, we observed a substantial signal for circularly polarized light. Figure 3 shows that now the current as a function of the angle φ can be well fitted by the dependencies

$$J_{x'} = \gamma P_{\rm circ} + \frac{\chi_1}{2} \sin 4\varphi, \quad J_{y'} = \chi_2 - \chi_3 \cos^2 2\varphi, \tag{3}$$

which follow from symmetry considerations for the miscut (111) Si transistors of the C_s point group. As compared with the exact (111) Si sample, the inclination leads to three distinctive features: (i) a current along the x' axis proportional to the radiation helicity $P_{\rm circ}$ is generated under normal incidence, (ii) the current component $J_{y'}$ acquires a polarization-independent contribution, and (iii) the absolute values of the coefficients χ_1, χ_3 describing the currents induced by linearly polarized light become different.

Now we show that the observed dependencies (1)–(3) are readily obtained by summing up the photocurrents $\boldsymbol{j}_\nu = e\boldsymbol{i}_\nu$ induced in individual valleys. Each valley ν ($\nu = X, Y, Z, X', Y'$, and Z', Fig. 1) has only one nontrivial symmetry element, the reflection $x_\nu \to -x_\nu$, described by the point group C_s. Here we use the following in-plane frame: the axis x_ν is perpendicular to the plane containing the principal valley axis and the channel normal $\boldsymbol{n}$ and the axis y_ν lies in this plane. Particularly, for $\boldsymbol{n} \parallel [111]$ the axes x_Z and y_Z coincide with $[\bar{1}10]$ and $[\bar{1}\bar{1}2]$, respectively. The current density emerging in the valley ν is phenomenologically given by[17]

$$\begin{aligned} j^{(\nu)}_{x_\nu}/I &= A(\theta_\nu)P_{\rm circ} + B(\theta_\nu)\left(e_{x_\nu}e^*_{y_\nu} + e_{y_\nu}e^*_{x_\nu}\right), \\ j^{(\nu)}_{y_\nu}/I &= C(\theta_\nu) + D(\theta_\nu)\left(|e_{x_\nu}|^2 - |e_{y_\nu}|^2\right), \end{aligned} \tag{4}$$

where I is the light intensity, $A(\theta_\nu)$, $B(\theta_\nu)$, $C(\theta_\nu)$, and $D(\theta_\nu)$ are polarization-independent coefficients, θ_ν is the angle between the normal $\boldsymbol{n}$ and the principal axis of the valley ν, and e_{x_ν} and e_{y_ν} are the projections of the polarization vector $\boldsymbol{e}$ on the x_ν and y_ν axes, respectively.

The total electric current is a sum of the single-valley contributions $\boldsymbol{j}^{(\nu)}$. In fact, the contributions due to the valleys X, X' (or Y, Y' and Z, Z') coincide so that the total photocurrent simplifies to

$$\boldsymbol{j} = 2 \sum_{\nu=X,Y,Z} \boldsymbol{j}^{(\nu)}. \tag{5}$$

By projecting all the partial vectors $\boldsymbol{j}^{(\nu)}$ on the transistor axes x and y (or x' and y') we obtain

$$\begin{aligned} j_x &= 2 \sum_{\nu=X,Y,Z} \left(j^{(\nu)}_{x_\nu} \cos\phi_\nu - j^{(\nu)}_{y_\nu} \sin\phi_\nu\right), \\ j_y &= 2 \sum_{\nu=X,Y,Z} \left(j^{(\nu)}_{x_\nu} \sin\phi_\nu + j^{(\nu)}_{y_\nu} \cos\phi_\nu\right), \end{aligned} \tag{6}$$

where ϕ_ν is the angle between the axes x_ν and x.

In the exact (111) Si-MOS structure all valleys are equivalent, $\theta_\nu = \Theta_0$ with $\cos\Theta_0 = 1/\sqrt{3}$ and the in-plane angles ϕ_ν are given by $\phi_X = -\phi_Y = 120^\circ, \phi_Z = 0$. Therefore, we derive

$$\begin{aligned} j_x/I &= 3(B_0 + D_0)(e_x e^*_y + e_y e^*_x), \\ j_y/I &= 3(B_0 + D_0)(|e_x|^2 - |e_y|^2), \end{aligned} \tag{7}$$

where $B_0 = B(\Theta_0)$ and $D_0 = D(\Theta_0)$. Equation (7) exactly reproduces the observed polarization dependencies (1) and (2) with the fitting parameter χ given by $3(B_0 + D_0)$. Thus, we conclude that while both circularly polarized and unpolarized radiation give rise to an electric currents $\boldsymbol{j}_\nu$ in all valleys, the total photocurrent can only be excited by linearly polarized light.

To describe the photocurrent in miscut structures, we introduce the polar angles Θ and Φ of the normal $\boldsymbol{n}$ in the Cartesian system [100], [010], [001]. If the channel normal $\boldsymbol{n}$ is close to [111], then the angles Θ and Φ are close to Θ_0 and $\Phi_0 = 45^\circ$, respectively. By expanding ϕ_ν, θ_ν in powers of $\delta\Theta = \Theta - \Theta_0$ and $\delta\Phi = \Phi - \Phi_0$ one can derive the expression for the photocurrent in miscut structures. In the approximation linear in $\delta\Theta$ and $\delta\Phi$, the total helicity-dependent current reduces to

$$\boldsymbol{j}^c/I = Q P_{\rm circ} \boldsymbol{l} \times \boldsymbol{n}, \tag{8}$$

where $Q = 3(A_0/\sqrt{2} + A_0')$, $A_0' = dA/d\theta|_{\theta=\Theta_0}$, and $\boldsymbol{l}$ is the unit vector along the crystallographic axis [111]. While deriving Eq. (8) we took into account that (i) for a fixed value of the total electron density the electron chemical potential is independent of $\delta\Theta$ and $\delta\Phi$; (ii) the angles θ_ν are expressed in terms of $\delta\Theta$, $\delta\Phi$ by $\theta_Z = \Theta_0 + \delta\Theta$ and $\theta_{X,Y} = \Theta_0 - \delta\Theta/2 \pm \delta\Phi/\sqrt{2}$; and (iii) the components $(\boldsymbol{l} \times \boldsymbol{n})_{x'}$ and $(\boldsymbol{l} \times \boldsymbol{n})_{y'}$ are given by $\delta\Theta$ and $\sqrt{2/3}\delta\Phi$, respectively. Equation (8) shows that the helicity-dependent photocurrent excited by normally incident radiation appears only in miscut structures and in the direction perpendicular to the inclination axis. This behavior is observed in all studied Si-MOSFETs [see Figs. 2(c) and 3]. In fact, the observation of the circular photogalvanic effect in miscut samples, where the equivalence of valleys is disturbed, demonstrates that photocurrents in individual valleys are efficiently generated.

The pure valley-orbit currents with zero net charge transfer can be classified according to their behavior under the symmetry operations. In (111)-oriented Si-MOS structures of the C_{3v} point group, the pure valley-orbit currents can belong to the irreducible representations A_1, A_2, and E. The scalar representation A_1 describes the pure valley-orbit current $j^{(A_1)}_{\text{valley}} = \sum_\nu j^{(\nu)}_{y_\nu}$; this current is excited by unpolarized radiation. The pseudoscalar representation A_2 describes the pure valley-orbit current $j^{(A_2)}_{\text{valley}} = \sum_\nu j^{(\nu)}_{x_\nu}$, which changes its sign upon reflection in any of the three mirror planes of the point group C_{3v}. The contribution $j^{(A_2)}_{\text{valley}}$ is induced by circularly polarized radiation [see Fig. 1(c)] and reverses its sign upon inversion of the photon helicity. Finally, the two-dimensional vector representation E describes the pure valley-orbit current with the components $j^{(E)}_{\text{valley},x} = (2j^{(Z)}_{x_Z} - j^{(X)}_{x_X} - j^{(Y)}_{x_Y}) + \sqrt{3}(j^{(X)}_{y_X} - j^{(Y)}_{y_Y})$ and $j^{(E)}_{\text{valley},y} = (-2j^{(Z)}_{y_Z} + j^{(X)}_{y_X} + j^{(Y)}_{y_Y}) + \sqrt{3}(j^{(X)}_{x_X} - j^{(Y)}_{x_Y})$. The polarization dependence of the pure valley-orbit current $\boldsymbol{j}^{(E)}_{\text{valley}}$ excited by normally incident radiation is given by Eq. (7) where D_0 is replaced by $-D_0$.

A complementary experiment to observe $j^{(A_2)}_{\text{valley}}$ is the generation of the second harmonic. Indeed, under normal incidence of the probe light, the dielectric polarization at the second harmonic frequency is given by

$$P_x^{(2)} = \chi^{(2)}_{xxy} 2\mathcal{E}_x\mathcal{E}_y + \chi^{(3)}_{xxx} j^{(A_2)}_{\text{valley}} \left(\mathcal{E}_x^2 - \mathcal{E}_y^2\right),$$
$$P_y^{(2)} = \chi^{(2)}_{xxy} \left(\mathcal{E}_x^2 - \mathcal{E}_y^2\right) - \chi^{(3)}_{xxx} j^{(A_2)}_{\text{valley}} 2\mathcal{E}_x\mathcal{E}_y,$$

where $\mathcal{E}$ is the probe electric-field amplitude, $\chi^{(2)}_{xxy} = \chi^{(2)}_{yxx} = -\chi^{(2)}_{yyy}$ is the second-order susceptibility of the equilibrium system, and $\chi^{(3)}_{xxx} = -\chi^{(3)}_{xyy} = -\chi^{(3)}_{yxy}$ is the third-order susceptibility, the second order in $\mathcal{E}$ and the first in $j^{(A_2)}_{\text{valley}}$. Note that the effect of the gate voltage on the generation of the second harmonic has been previously observed in (001) Si-MOSFETs.[26] Another possibility is the *orbital* Kerr or Faraday rotation of the probe beam caused by the pure valley-orbit current with the rotation angle $\Phi \propto j^{(A_2)}_{\text{valley}}$, similar to the spin Kerr or Faraday effect.

To summarize, we demonstrate that pure valley-orbit currents can be generated by optical excitation of multivalley semiconductors. The appearance of a pure valley-orbit current is a specific feature of semiconductors with several equivalent valleys such as graphene, carbon nanotubes, and silicon, the latter being the focus of our work. The electron fluxes in valleys can be individually controlled by simple means, namely by variation of light polarization or by the disturbance of the valleys equivalence. The latter can be achieved, for example, by the application of strain. A controllable way of a selective occupation of valleys and the generation of pure valley-orbit currents are key ingredients for valleytronics aimed at the development of novel solid-state devices.

This work was supported by the German Research Foundation (DFG) in the framework of the Priority Program 1459 "Graphene", Linkage Grant of IB of BMBF at DLR, RFBR, Russian Ministry of Education and Sciences, and "Dynasty" Foundation ICFPM.

[1] I. Žutić *et al.*, Rev. Mod. Phys. **76**, 323 (2004).
[2] S. A. Tarasenko and E. L. Ivchenko, Pis'ma Zh. Eksp. Teor. Fiz. **81**, 292 (2005) [JETP Lett. **81**, 231 (2005)].
[3] A. Rycerz *et al.*, Nat. Phys. **3**, 172 (2007).
[4] R. N. McFarland, T. M. Kott, L. Sun, K. Eng, and B. E. Kane, Phys. Rev. B **80**, 161310 (2009).
[5] J. L. Garcia-Pomar, A. Cortijo, and M. Nieto-Vesperinas, Phys. Rev. Lett. **100**, 236801 (2008).
[6] A. S. Moskalenko and J. Berakdar, Phys. Rev. B **80**, 193407 (2009).
[7] M. I. Dyakonov (ed.), *Spin Physics in Semiconductors* (Springer, New York, 2008).
[8] A. A. Kaplyanskii *et al.*, Solid State Commun. **20**, 27 (1976).
[9] R. D. R. Bhat, F. Nastos, A. Najmaie, and J. E. Sipe, Phys. Rev. Lett. **94**, 96603 (2005).
[10] S. D. Ganichev *et al.*, Nat. Phys. **2**, 609 (2006).
[11] H. Zhao, X. Pan, A. L. Smirl, R. D. R. Bhat, A. Najmaie, J. E. Sipe, and H. M. van Driel, Phys. Rev. B **72**, 201302 (2005).
[12] E. L. Ivchenko and S. A. Tarasenko, Semicond. Sci. Technol. **23**, 114007 (2008).
[13] C. L. Kane and E. J. Mele, Phys. Rev. Lett. **95**, 146802 (2005).
[14] M. König *et al.*, Science **318**, 766 (2007).
[15] T. Cole and B. D. McCombe, Phys. Rev. B **29**, 3180 (1984).
[16] L. I. Magarill and M. V. Entin, Fiz. Tverd. Tela **31**, 37 (1989) [Sov. Phys. Solid State **31**, 1299 (1989)].
[17] J. Karch *et al.*, J. Phys. Condens. Matter **22**, 355307 (2010).
[18] S. A. Tarasenko, Phys. Rev. B **83**, 035313 (2011).
[19] P. Olbrich, S. A. Tarasenko, C. Reitmaier, J. Karch, D. Plohmann, Z. D. Kvon, and S. D. Ganichev, Phys. Rev. B **79**, 121302 (2009).
[20] G. M. Gusev *et al.*, JETP Lett. **40**, 1056 (1984).
[21] A. A. Kapustin, A. A. Shashkin, V. T. Dolgopolov, M. Goiran, H. Rakoto, and Z. D. Kvon, Phys. Rev. B **79**, 205314 (2009).
[22] T. Ando *et al.*, Rev. Mod. Phys. **54**, 437 (1982).
[23] S. D. Ganichev, S. A. Emel'yanov, and I. D. Yaroshetskii, Sov. Phys. JETP Lett. **35**, 368 (1982).
[24] S. D. Ganichev and W. Prettl, *Intense Terahertz Excitation of Semiconductors* (Oxford University Press, Oxford, 2006).
[25] W. Weber *et al.*, Phys. Rev. B **77**, 245304 (2008).
[26] J. Fang and G. P. Li, Appl. Phys. Lett. **75**, 3506 (1999).